

Wannier-Stark states and Bloch oscillations in the honeycomb lattice

Andrey R. Kolovsky^{1,2} and Evgeny N. Bulgakov¹

¹*Kirensky Institute of Physics, 660036 Krasnoyarsk, Russia*

²*Siberian Federal University, 660041 Krasnoyarsk, Russia*

(Received 10 November 2012; published 4 March 2013)

We study a quantum particle in a tilted honeycomb lattice in the tight-binding approximation. First we discuss the particle eigenstates, i.e., the stationary Wannier-Stark states. These states are proved to be extended states for the rational directions of the static field and localized states for the irrational directions. We find energy bands of the extended states and analyze the localized states. It is shown, in particular, that the localized honeycomb Wannier-Stark states are chaotic states with irregular dependence of the localization length on the static field magnitude. Second we discuss Bloch oscillations of the quantum particle. Irregular Bloch oscillations for irrational directions are observed.

DOI: [10.1103/PhysRevA.87.033602](https://doi.org/10.1103/PhysRevA.87.033602)

PACS number(s): 03.75.Lm, 72.10.Bg

I. INTRODUCTION

Wannier-Stark states (WS states) are eigenstates of quantum particle in a tilted lattice, i.e., in the presence of a static field. Strictly speaking WS-states are resonances and have complex energies. However, for weak static fields they can be approximated by the stationary states with real energies (the single-band and tight-binding approximations). In the past two decades WS states and related problems of Bloch oscillations (BO) and interband Landau-Zener tunneling (LZ tunneling) were readdressed in a number of fascinating laboratory experiments with cold atoms in (quasi-) one-dimensional (1D) optical lattices and the light in 1D arrays of optical wave guides, see Refs. [1–8] to cite a few of dozens of relevant papers. These experiments stimulated theoretical studies that resulted in essential progress in the theory of WS states in one-dimensional systems, see Ref. [9] for a review.

An interesting extension of the theory of 1D WS states refers to 2D tilted lattices [10–12]. It was argued in Ref. [10] and confirmed later on in the experiment [7] that WS states in a 2D lattice are sensitive to the direction of the static field relative to primary axes of the lattice. Unfortunately, for square lattices considered in the above-cited papers this effect is seen only in the strong-field regime, where the metastable nature of WS states plays major role. In the present work we analyze WS states and BO for a quantum particle in a honeycomb lattice. We will show that for this lattice geometry the nonanalytic angular dependence of WS states is well pronounced already in the weak-field regime, where the metastable WS states can be approximated by the stationary states. This feature of the stationary honeycomb WS states has direct consequences for Bloch dynamics of the system that becomes qualitatively different for rational and irrational field directions defined later on in the text.

It should be mentioned that BO in the honeycomb lattice were addressed earlier with respect to conductivity of graphene nanoribbons [13,14]. However, in these works the electric field was aligned with the ribbon axis and, thus, the alignment effects were not discussed. The other related problem is a Bose-Einstein condensate of cold atoms in the square optical lattice in the presence of an effective spin-orbit coupling. It is known that the spin-orbit coupling results in the Bloch dispersion relation similar to that for a quantum particle in

the honeycomb lattice [15,16]. Bloch dynamics of a spin-orbit-coupled condensate was analyzed in Ref. [15] for the particular case where static field was aligned with the lattice primary axis. Because of the above-mentioned similarity between two systems, results of the present work can be also used to describe the Bloch dynamic of spin-orbit-coupled Bose-Einstein condensates for arbitrary directions of an external field.

This paper consists of two parts devoted to analytical and numerical analysis of WS states, Sec. II, and BO of a quantum particle in the honeycomb lattices, Sec. III. The main results of the work are summarized in Sec. IV.

II. HONEYCOMB WANNIER-STARK STATE

In the standard presentation with two sublattices the tight-binding Hamiltonian of a quantum particle in the honeycomb lattice reads

$$H_0 = -J \sum_{\mathbf{R}} \left(\sum_{j=1}^3 b_{\mathbf{R}+\mathbf{r}_j}^\dagger a_{\mathbf{R}} + \text{H.c.} \right), \quad (1)$$

where J is the hopping matrix element, \mathbf{R} denote coordinates of A sites, and \mathbf{r}_j are three vectors that point from a A site to the nearest B sites. If a static field is present, this Hamiltonian should be complemented with the Stark term,

$$H = H_0 + \sum_{\mathbf{R}} (\mathbf{F}, \mathbf{R}) a_{\mathbf{R}}^\dagger a_{\mathbf{R}} + \sum_{\mathbf{R}'} (\mathbf{F}, \mathbf{R}') b_{\mathbf{R}'}^\dagger b_{\mathbf{R}'}, \quad (2)$$

where \mathbf{F} is the vector of the static field and \mathbf{R} and \mathbf{R}' are coordinates of the A and B sites, respectively. We are interested in the eigenstates of the Hamiltonian (2), i.e., in the stationary honeycomb WS states.

We begin with recalling a general result concerning the structure of WS states in a two-dimensional lattice of arbitrary geometry: For the field \mathbf{F} parallel to a vector pointing from one lattice site to any other site WS states are extended states in the direction orthogonal to \mathbf{F} . These field directions can be labeled by two coprime numbers r and q and for this reason are termed rational directions. For example, for the square lattice the rational directions are given by $F_y/F_x = r/q$ or

$$\tan \theta = r/q, \quad (3)$$

while for the honeycomb lattice these are

$$\tan \theta = \sqrt{3} \frac{q-r}{q+r}. \quad (4)$$

The spectrum of WS states for a rational direction (r, q) consists of infinite number of equally spaced energy bands. A particular feature of the square lattice and other simple lattices (like, for example, the triangular lattice [17]) is that these energy bands are flat for almost all rational directions. Because of this feature there is no qualitative difference between rational and irrational directions for the square lattice in the tight-binding approximation. In what follows we show that the Wannier-Stark energy bands of the honeycomb lattice have finite widths already in the tight-binding approximation. This makes a crucial difference between the honeycomb lattice and the square or triangular lattices, as well as between rational and irrational directions for the honeycomb lattice.

A. Rational field directions

For rational directions WS states in the honeycomb lattice are labeled by the ladder number n , the transverse quasimomentum κ , and the sublattice index i . Correspondingly, the energy spectrum is given by

$$E_n^{(i)}(\kappa) = E_0^{(i)} + d\tilde{F}n + \epsilon^{(i)}(\kappa), \quad (5)$$

where

$$d = \frac{1}{\sqrt{r^2 + q^2}}, \quad \tilde{F} = \frac{3F}{2d} \frac{1}{\sqrt{r^2 - rq + q^2}}, \quad (6)$$

and $\epsilon^{(i)}(\kappa)$ is a periodic function of κ . We calculated the spectrum (5) by adopting the method of Refs. [19–21]. In brief, we map the honeycomb lattice into a square lattice with two sublattices. For this square lattice the static field is characterized by the vector $\tilde{\mathbf{F}}$ and the rational directions are given by $\tilde{F}_y/\tilde{F}_x = r/q$. Next we introduce another square lattice of the period d , which includes the previous lattice as a sublattice, and rotate it to align its x axis with the vector $\tilde{\mathbf{F}}$. Finally we use substitution where the wave function is a plane wave along the y axis. After this sequence of transformations we end up with the system of two coupled equations,

$$\begin{aligned} & -J(e^{-iq\kappa d}\psi_{j-r}^B + e^{ir\kappa d}\psi_{j-q}^B + e^{i(r-q)\kappa d}\psi_{j-r-q}^B) \\ & + (d\tilde{F}j + E_0^A)\psi_j^A = E\psi_j^A, \\ & -J(e^{iq\kappa d}\psi_{j+r}^A + e^{-ir\kappa d}\psi_{j+q}^A + e^{i(q-r)\kappa d}\psi_{j+r+q}^A) \\ & + (d\tilde{F}j + E_0^B)\psi_j^B = E\psi_j^B, \end{aligned} \quad (7)$$

where $E_0^B = (2/3)(r+q)d\tilde{F}$ if one sets $E_0^A = 0$.

We solved Eq. (7) numerically for different F and (r, q) . Without any loss of generality one can restrict θ to the interval $0 \leq \theta < \pi/3$, which means $q > r \geq 0$. Examples of the spectrum (5) are given in Fig. 1 where the chosen energy intervals include three bands with $i = 1$ and three bands with $i = 2$. In addition to Figs. 1 and 2 shows the width of the energy bands,

$$\Delta = \max_{\kappa} \epsilon(\kappa) - \min_{\kappa} \epsilon(\kappa), \quad (8)$$

as the function of F for the field direction $\theta = \pi/6$ (asterisk) and some other directions. [Since Δ is independent of i ,

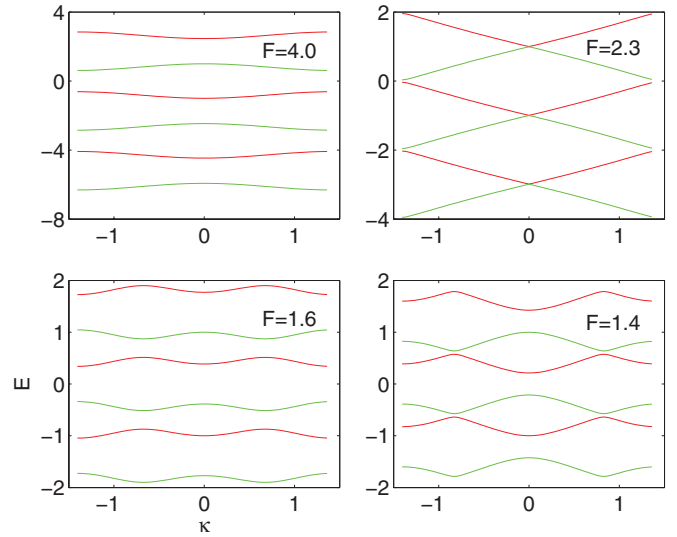


FIG. 1. (Color online) Fragments of the spectrum (5) for $(r, q) = (1, 2)$ or $\theta = \pi/6$ and different field magnitude F . The value of the hopping matrix element J , which defines the energy scale, and the lattice period are set to unity.

we drop the sublattice index in Eq. (8).] From the depicted numerical data one draws the following conclusions: The bands are well separated only in the limit of large F ; with decrease of F the band width Δ monotonically grows while the distance $d\tilde{F}$ between bands monotonically decreases and, for some $F_{cr} \sim J$, the bands almost touch each other. At this critical field magnitude the width Δ takes its maximal value; After reaching the maximum Δ shows monotonic decrease, where bands become flatter; this decrease is followed by erratic oscillations of the band width for small F . We note that in this region of small F the quantity (8) is not sufficient to characterize the spectrum because of rather complicated band pattern with many avoided crossings.

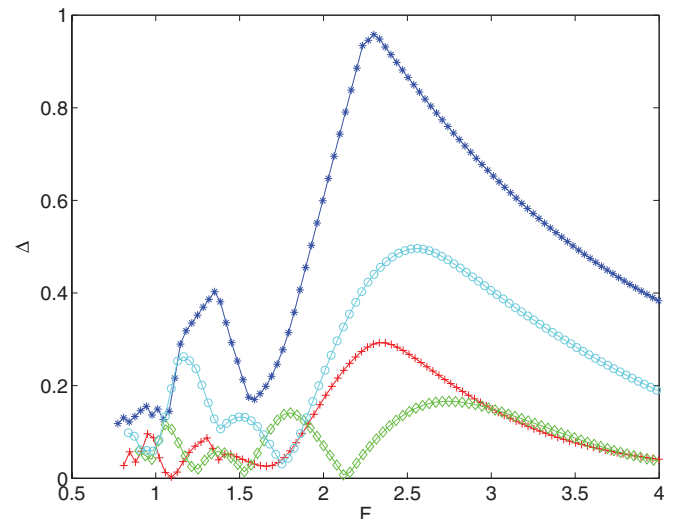


FIG. 2. (Color online) The band width (8) as the function of the field magnitude for $(r, q) = (1, 2)$, asterisks, $(1, 3)$, circles, $(1, 5)$, diamonds, and $(2, 5)$, crosses.

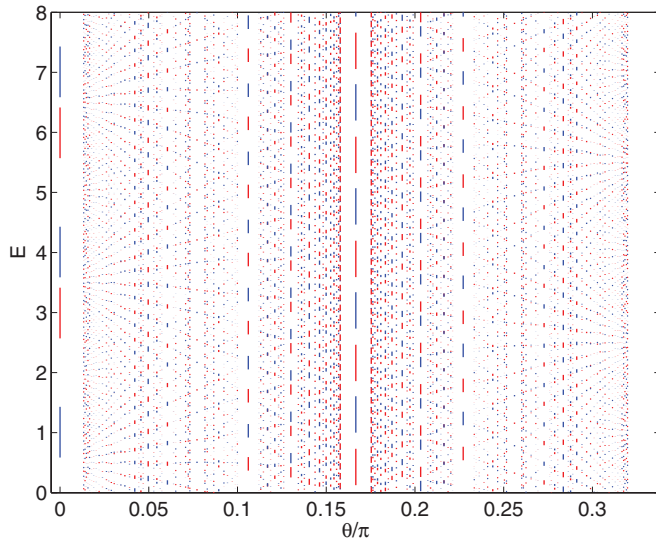


FIG. 3. (Color online) Widths of the energy bands for different rational directions for $F = 2$.

We also studied the asymptotic behavior of Δ for $F \rightarrow \infty$. Our numerical analysis reveals the dependence

$$\Delta \sim \frac{1}{F^\nu}, \quad (9)$$

where ν increases with the increase of the denominator $r + q$ in Eq. (4). For example, $\nu = 1$ for $(r, q) = (1, 1)$, $\nu = 2$ for $(r, q) = (1, 2)$, etc. This result resembles that for the band widths of the Landau-Stark states (eigenstates of a quantum particle in the Hall configuration) in the square lattice [21]. We believe that the power $\nu = \nu(r, q)$ in Eq. (9) can be calculated analytically by adopting the perturbative approach of Ref. [21].

Dependence of the band width Δ on the field direction θ is depicted in Fig. 3, which presents the energy spectrum of the system (2) in the form of Hofstadter's butterfly. Namely, the figure shows energy bands for angles (4) with $1 < r \leq q \leq 21$, where the red (dark gray) and green (light gray) colors correspond to $i = 1$ and $i = 2$, respectively. It is seen in Fig. 3 that the band widths progressively decrease with increase of r and q . Together with the estimate (9) this means that for irrational directions the spectrum is pure point and, hence, WS states are localized states.

B. Irrational field directions

First we check that WS states for irrational directions are localized states. In Fig. 4 we compare two eigenstates of the Hamiltonian (2) with nearly the same energy for a rational $\theta = \pi/2 \approx 1.57$ (equivalent to $\theta = \pi/6$) and irrational $\theta = 3 - \pi/2 \approx 1.43$. The figure shows the integrated probabilities $\rho_y = \int |\Psi(\mathbf{R})|^2 dx$, dashed line, and $\rho_x = \int |\Psi(\mathbf{R})|^2 dy$, solid line. (From now on we do not distinguish A and B sites.) For rational θ the WS state is seen to be an extended state in the direction orthogonal to \mathbf{F} , while for irrational θ it is localized in both directions.

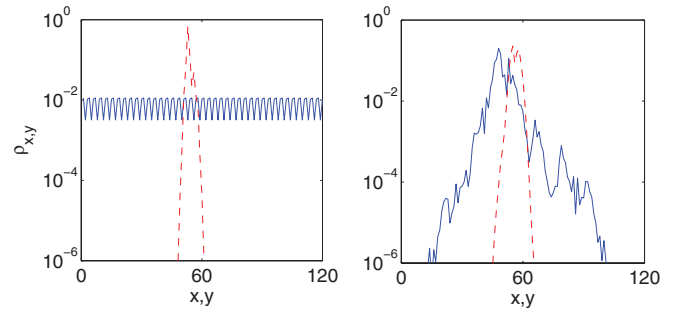


FIG. 4. (Color online) Examples of extended (left panel, $\theta = \pi/2$) and localized (right panel, $\theta = 3 - \pi/2$) WS states with nearly the same energies. The dashed and solid lines show integrated probabilities along and across the field, respectively. The field magnitude $F = 1$.

An important characteristic of the localized WS states is their participation ratio,

$$P = \left(\sum_{\mathbf{R}} |\Psi(\mathbf{R})|^4 \right)^{-1}, \quad (10)$$

which indicates how many sites are occupied by a given state. We note that the participation ratio (10) is the same for every WS state because different WS states are related to each other by translations. In the other words, one can obtain the complete set of WS states from one state (or two states, if the lattice consists of two sublattices) by translating it across the lattice.

A remarkable feature of the honeycomb WS states is that their participation ratio wildly oscillates if F is varied. The physics behind these oscillations is the following. Similar to the case considered in the previous subsection the (now discrete) spectrum of WS state consists of two subsets that can be labeled by the subband index i or, what is the same, by the letters A and B. Correspondingly, we have two families of WS states [22]. When F is varied the energy levels of A and B states nonmonotonically move on the energy axis. If two levels of different symmetry come close to each other they develop an avoided crossing where the A and B states hybridize. As a consequence of the hybridization the function $P = P(F)$ shows a local maximum, see inset in Fig. 5. It should be mentioned that to resolve all local peaks of $P(F)$ (i.e., all avoided crossings in the spectrum) the step over F or, more precisely, over $z = 1/F$ should be infinitesimally small. Figure 5 shows the function $P = P(F)$ for a moderate step where only large peaks are resolved. Erratic oscillations with increasing density of peaks are clearly seen. This figure also reveals the expected average growth of the participation ratio when F is decreased.

It is interesting to compare the localized honeycomb WS states against the analytic results for the simple square lattice,

$$\Psi(\mathbf{R}) = \mathcal{J}_{l-n}(J/F_x) \mathcal{J}_{m-k}(J/F_y), \quad \mathbf{R} = (l, m) \quad (11)$$

[here $\mathcal{J}_n(z)$ are the Bessel functions of the first kind]. The square lattice has only one family of WS states and, correspondingly, the energy levels show no avoided crossings. Participation ration of the states (11) is depicted in Fig. 5 by the thick line. Comparing two curves we conclude that WS state in the honeycomb lattice are irregular or chaotic states,

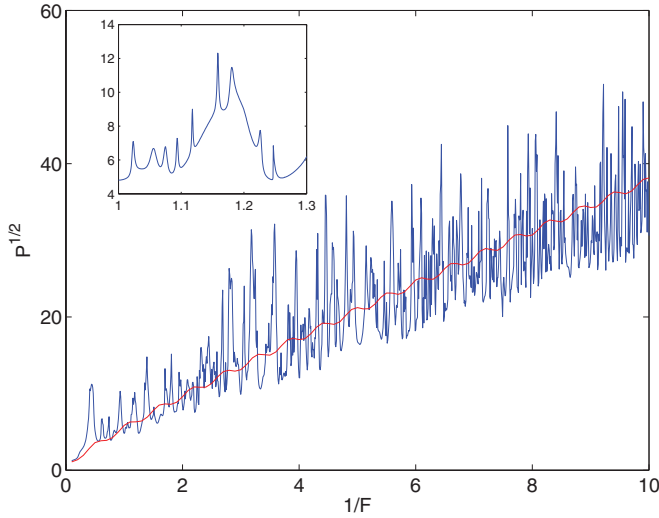


FIG. 5. (Color online) Localization length of WS states for irrational direction $\theta = 3 - \pi/2$. The thick and thin lines show the square root of the participation ratio (10) for the square and honeycomb lattices, respectively. The inset zooms into the region $1/F \approx 1$.

which are sensitive to variations of the system parameters [23]. The statistical analysis of these states in spirit of the random matrix theory will be presented elsewhere.

III. BLOCH DYNAMICS

To study Bloch dynamics of the system (2) it is convenient to use the interaction representation with respect to the Stark term. This results in the time-dependent Hamiltonian

$$H(t) = -J \sum_{\mathbf{R}} \left(\sum_{j=1}^3 b_{\mathbf{R}+\mathbf{r}_j}^\dagger a_{\mathbf{R}} e^{i\omega_j t} + \text{H.c.} \right), \quad (12)$$

where $\omega_j = (\mathbf{F}, \mathbf{r}_j)$ are the Bloch frequencies. Notice that the Hamiltonian (12) commutes with the translation operator. Thus, when considering translation-invariant solutions of the Schrödinger equation, we can impose periodic boundary conditions.

A. Delocalized initial state

Consider initial state of the system $\Psi(\mathbf{R}, t=0)$ given by an eigenstate of the Hamiltonian (1), i.e., by the Bloch wave $\Psi_{\mathbf{k}}(\mathbf{R})$ with the quasimomentum \mathbf{k} . Then the time evolution of this state is naively expected to obey the equation $\Psi(\mathbf{R}, t) \sim \Psi_{\mathbf{k}+\mathbf{F}t}(\mathbf{R})$, that is known as the acceleration theorem. This simple Bloch dynamics, however, is complicated by the fact that the spectrum of H_0 consist of two sub-bands,

$$E(\mathbf{k}) = \pm J \sqrt{1 + 4 \cos^2 \left(\frac{\sqrt{3}}{2} k_y \right) + 4 \cos \left(\frac{\sqrt{3}}{2} k_y \right) \cos \left(\frac{3}{2} k_x \right)}, \quad (13)$$

with the energy gap vanishing at the Dirac points. Thus one generally can not avoid interband LZ tunneling and the actual

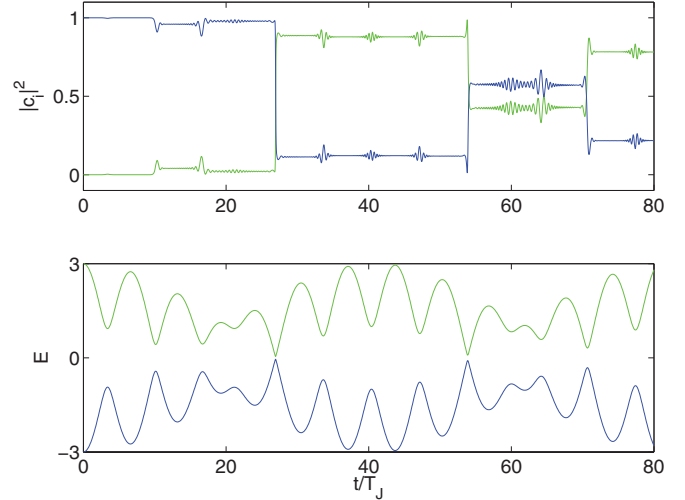


FIG. 6. (Color online) Populations of two Bloch subbands as the functions of time, upper panel, and the energies (13) for $\mathbf{k}' = \mathbf{F}t$, lower panel. Parameters are $\theta = \pi - 3$ and $F = 0.1$. Initial condition corresponds to the ground state of the system for $F = 0$, i.e., to the Bloch wave with zero quasimomentum.

time evolution is given by the equation

$$\Psi(\mathbf{R}, t) = \sum_{i=1}^2 c_i(t) \Psi_{\mathbf{k}+\mathbf{F}t}^{(i)}(\mathbf{R}), \quad (14)$$

where i is the Bloch subband index and the coefficients $c_i(t)$ obeys the equation

$$i \frac{d\mathbf{c}}{dt} = -J \begin{pmatrix} 0 & f(t) \\ f^*(t) & 0 \end{pmatrix} \mathbf{c}, \quad (15)$$

$$f(t) = \sum_{j=1}^3 \exp(i\mathbf{k}\mathbf{r}_j + i\mathbf{F}\mathbf{r}_j t).$$

[Notice that for $F = 0$ Eq. (15) defines the energy spectrum (13).] The upper panel in Fig. 6 shows typical dynamics of the coefficients $c_i(t)$ and the lower panel depicts the energies (13) at $\mathbf{k}' = \mathbf{k} + \mathbf{F}t$. It is seen that LZ tunneling predominantly takes place when \mathbf{k}' appears in the vicinity of Dirac points.

It should be stressed that the discussed Landau-Zener transitions may completely smear the periodic or quasiperiodic dynamics of quantum observables that is usually associated with BO. In what follows we focus on dynamics of the projection of the mean momentum onto the field direction:

$$p(t) = \sum_{j=1}^3 \frac{\omega_j}{F} p_j(t), \quad (16)$$

$$p_j(t) = \text{Im} \langle \Psi(t) | J \sum_{\mathbf{R}} b_{\mathbf{R}+\mathbf{r}_j}^\dagger a_{\mathbf{R}} e^{i\omega_j t} | \Psi(t) \rangle.$$

Figure 7 compares $p(t)$ for $F = 0.1$ and $\theta = 0$ (upper panel) and $\theta = \pi - 3$ (lower panel). In the former case the particle trajectory in the (quasi)momentum space goes between Dirac points and LZ tunneling can be neglected for chosen F . Thus the upper sub-band remains unpopulated and we observe nice periodic oscillations of the mean momentum which reproduce

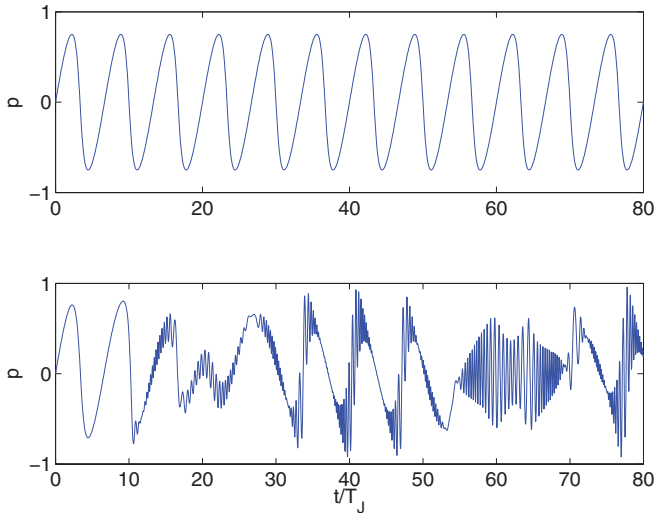


FIG. 7. (Color online) Projection of the mean momentum on the field direction as the function of time for $F = 0.1$ and $\theta = 0$, upper panel, and $\theta = \pi - 3$, lower panel.

the derivative of the dispersion relation (13) along the line $\mathbf{k} = \mathbf{F}t$,

$$p(t) = \frac{1}{F} E'(\mathbf{F}t). \quad (17)$$

In the latter case the upper sub-band gets populated independent of how small F is. As a consequence, $p(t)$ shows irregular oscillations where one hardly recognizes the former periodic BO.

To clarify further the difference between regular and irregular oscillations we display in Fig. 8 the Fourier spectrum of $p(t)$, which is calculated according to the equation

$$p(v) = \frac{1}{T} \int_0^T p(t) e^{ivt} dt. \quad (18)$$

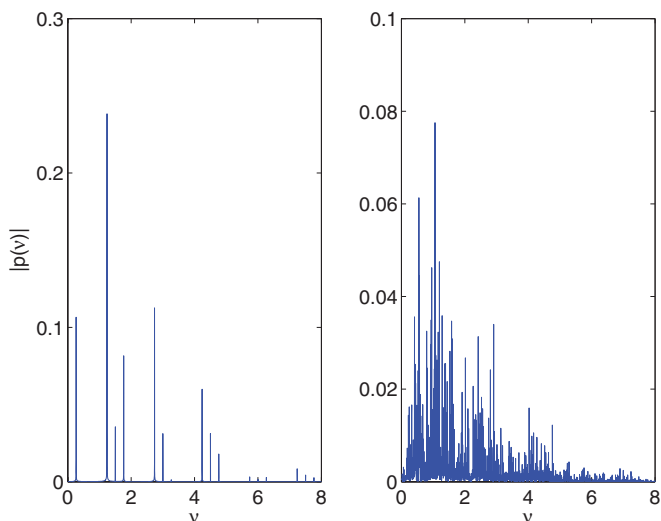


FIG. 8. (Color online) Fourier spectrum of $p(t)$ for the parameters of Fig. 7 yet $F = 1$. Since the spectrum is symmetric with respect to the origin, only positive part of the spectrum is shown.

By progressively increasing T in Eq. (18) we reveal the discrete nature of the Fourier spectrum. Thus, independent of the field direction, dynamic of the mean momentum (or any other observable) is a quasiperiodic process. The difference is in the complexity of this quasiperiodic process. For rational directions, where the Bloch frequencies ω_j in the governing equation (12) are commensurate, $p(v)$ consists of few well-separated peaks, see Fig. 8(a). On the contrary, for irrational directions, where the frequencies ω_j are incommensurate, the spectrum is dense and resembles that of a random process, see Fig. 8(b). This difference becomes especially apparent if we consider the limit $F \rightarrow 0$. As mentioned above, in this limit and for rational directions LZ tunneling can be neglected and $p(t)$ converges to the periodic function (17). For irrational directions, due to the presence of Dirac cones, LZ tunneling is always present in the system and $p(t)$ does not converge to Eq. (17) or any other simple function.

B. Localized initial state

Wave-packet Bloch dynamics in a 2D lattice with two sub-bands was considered earlier in Refs. [11,12]. The wave packet was found to have a tendency to spread in the direction orthogonal to \mathbf{F} , while in the direction parallel to \mathbf{F} it shows oscillatory dynamics. In this work we consider the limiting case of a localized initial packet where only one site is populated at $t = 0$. Also we will discuss dynamics in terms of WS states instead of discussing it in terms of Bloch states as it was done in the above cited papers. To describe the wave-packet time evolution we introduce the time-dependent analog of Eq. (10),

$$P(t) = \left(\sum_{\mathbf{R}} |\Psi(\mathbf{R}, t)|^4 \right)^{-1}. \quad (19)$$

According to the results of Sec. II we expect qualitatively different dynamics of the participation ratio (19) for rational and irrational field directions.

The dashed line in Fig. 9 shows $P(t)$ for $F = 1$ and rational direction $\theta = 0$. The participation ratio exhibits oscillatory dynamics superimposed with a linear increase in the mean value. This linear increase is due to ballistic spreading of the packet in the direction orthogonal to \mathbf{F} . The rate of ballistic spreading is obviously defined by the width Δ of the Wannier-Stark bands, while the characteristic frequency of oscillations is given by the distance between neighboring Wannier-Stark bands.

The case of irrational direction $\theta = \pi - 3$ is depicted by the solid line in Fig. 9. Now $P(t)$ saturates at some level defined by the localization length of the honeycomb WS states. The wave-packet simulations also confirm $1/F^2$ scaling law for the saturation level of $P(t)$ that follows from the $1/F^2$ scaling law for participation ratio of the localized honeycomb WS states.

We would like to mention that the observed saturation of $P(t)$ can be viewed as a dynamical localization. This phenomenon was first observed for the quantum kicked rotor [24] and then found in many other driven systems. Since the effect of a static field amounts to (quasi)periodic driving of the system with Bloch frequencies, our system of interest obviously belongs to the class of quantum driven systems.

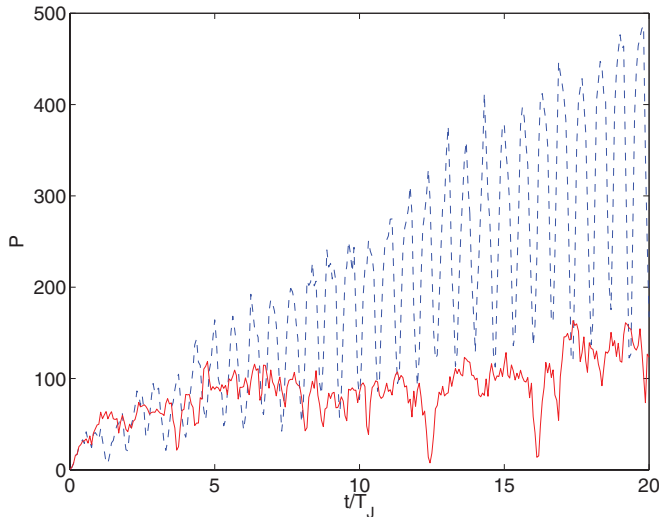


FIG. 9. (Color online) Participation ratio (19) for $\theta = 0$ (dashed line) and $\theta = \pi - 3$ (solid line). The initial condition corresponds to population of a single site in the center of the lattice. The value of the static force $F = 1$.

The dynamical localization in the kicked rotor was explained in Ref. [25] by appealing to the Anderson localization for a quantum particle in a random potential. In our case the Aubry-André model [26], which describes the particle localization in a quasiperiodic potential, seems to be more relevant than the Anderson model. It is an open problem to prove the saturation of $P(t)$ for irrational directions (incommensurate Bloch frequencies) from the viewpoint of the dynamical localization.

To conclude this section we mention that for some system parameters we observed rather exotic wave-packet dynamics that essentially differs from the above discussed general situation. One example is $\theta = \pi/6$ and $F = 2.3$. As it is seen from Fig. 1(b), for these parameters the energy bands are straight lines with exception of vicinities of the points $\kappa = 0$ and $\kappa = \pi/\sqrt{5}$. This mimics the dispersion relation of a relativistic particle in one dimension—the problem that attracted much attention in recent years [16,27–29]. Notice that the reduction to one dimension is provided by the Stark localization and, hence, no confinement potentials are required.

IV. CONCLUSION

We calculated WS states of a quantum particle in a tilted honeycomb lattice and compared them with WS states in

the tilted square lattice that are known analytically. The comparison is done for both rational and irrational tilts, i.e., rational and irrational directions of a static field \mathbf{F} .

For rational directions of the field defined in Eqs. (3) and (4) the energies of WS states form energy bands. For the square lattice these bands have zero width, excluding the case where \mathbf{F} is aligned with one of two primary axes. This prohibits any transport in the system if the vector \mathbf{F} is misaligned with a primary axis. Unlike this situation, for the honeycomb lattice the bands have finite width for any rational direction. If the condition (4) is fulfilled, an initially localized wave packet spreads in the direction orthogonal to \mathbf{F} [30]. We note in passing that this result provides an alternative explanation of findings of the numerical experiment [31], where dynamics of ultracold atoms in the parabolic square and hexagonal lattices were compared.

For irrational directions of the field the energy spectrum of WS states is discrete and, hence, they are localized states. We found the localization length of the honeycomb WS states, which we define as the square root of the participation ratio (10), to grow in average as $1/F$, i.e., in the same way as for the square lattice. However, in a smaller scale the localization length shows large fluctuations that do not present in the case of square lattice. This observation motivates us to put forward a hypothesis about irregular (chaotic) nature of the honeycomb WS states. This hypothesis is further supported by the irregular character of BO for irrational directions of the static field.

The results of this work can be verified in laboratory experiments with cold atoms in honeycomb optical lattices [16,29,31], honeycomb photonic crystals [32,33], and microwave billiards with honeycomb array of scatterers [34]. The common feature of these systems is that they offer direct visualization of the wave function. Another direction is ballistic conductivity of the graphene sheets. It is expected that the reported nonanalytic angular dependence of WS states could strongly affect the conductivity. We reserve the latter problem for future studies.

ACKNOWLEDGMENTS

The authors express their gratitude to D. N. Maksimov for useful remarks and acknowledge financial support of Russian Academy of Sciences through the SB RAS integration Project No. 29 (Dynamics of atomic Bose-Einstein condensates in optical lattices) and the Russian Foundation for Basic Research (RFBR) Project No. 12-02-00094 (Tunneling of the macroscopic quantum states).

[1] M. Ben Dahan, E. Peik, J. Reichel, Y. Castin, and C. Salomon, *Phys. Rev. Lett.* **76**, 4508 (1996).
 [2] M. G. Raizen, C. Salomon, and Qian Niu, *Phys. Today* **50**, 30 (1997).
 [3] O. Morsch, J. H. Müller, M. Cristiani, D. Ciampini, and E. Arimondo, *Phys. Rev. Lett.* **87**, 140402 (2001).

[4] S. Kling, T. Salger, C. Grossert, and M. Weitz, *Phys. Rev. Lett.* **105**, 215301 (2010).
 [5] T. Pertsch, P. Dannberg, W. Elflein, A. Bräuer, and F. Lederer, *Phys. Rev. Lett.* **83**, 4752 (1999).
 [6] R. Morandotti, U. Peschel, J. S. Aitchison, H. S. Eisenberg, and Y. Silberberg, *Phys. Rev. Lett.* **83**, 4756 (1999).

- [7] H. Trompeter, W. Krolikowski, D. N. Neshev, A. S. Desyatnikov, A. A. Sukhorukov, Y. S. Kivshar, T. Pertsch, U. Peschel, and F. Lederer, *Phys. Rev. Lett.* **96**, 053903 (2006).
- [8] F. Dreisow, A. Szameit, M. Heinrich, T. Pertsch, S. Nolte, A. Tünnermann, and S. Longhi, *Phys. Rev. Lett.* **102**, 076802 (2009).
- [9] M. Glück, A. R. Kolovsky, and H. J. Korsch, *Phys. Rep.* **366**, 103 (2002).
- [10] M. Glück, F. Keck, A. R. Kolovsky, and H. J. Korsch, *Phys. Rev. Lett.* **86**, 3116 (2001).
- [11] A. R. Kolovsky and H. J. Korsch, *Phys. Rev. A* **67**, 063601 (2003).
- [12] D. Witthaut, F. Keck, H. J. Korsch, and S. Mossmann, *New J. Phys.* **6**, 41 (2004).
- [13] G. J. Ferreira, M. N. Leuenberger, D. Loss, and J. C. Egues, *Phys. Rev. B* **84**, 125453 (2011).
- [14] V. Krueckl and K. Richter, *Phys. Rev. B* **85**, 115433 (2012).
- [15] J. Larson and E. Sjöqvist, *Phys. Rev. A* **82**, 043620 (2010).
- [16] Dan-wei Zhang, Zi-dan Wang, and Shi-liang Zhu, *Front. Phys.* **7**, 31 (2012).
- [17] The triangular lattice can be mapped into a square lattice with additional diagonal hopping. Then, by using the result of Ref. [18], one can prove that the energy bands are flat for all rational directions excluding $\theta = \pm\pi/6$ and $\theta = \pi/2$.
- [18] F. Keck and H. J. Korsch, *J. Phys. A: Math. Gen.* **35**, L105 (2002).
- [19] T. Nakanishi, T. Ohtsuki, and M. Saitoh, *J. Phys. Soc. Jpn.* **62**, 2773 (1993).
- [20] T. Nakanishi, T. Ohtsuki, and M. Saitoh, *J. Phys. Soc. Jpn.* **64**, 2092 (1995).
- [21] A. R. Kolovsky, I. Chesnokov, and G. Mantica, *Phys. Rev. E* **86**, 041146 (2012).
- [22] In fact, these states are related to each other by a symmetry transformation and, hence, have the same P .
- [23] In a narrow sense the term chaotic states means eigenstates of a quantum system that has chaotic dynamics in the classical limit. These states have no explicit analytical form and are known to be very sensitive to variations of the system parameters. Since our system has no classical counterpart, we use the term chaotic states in a wide sense, to stress the absence of an explicit expression for the wave functions and sensitivity to variation of the parameters.
- [24] G. Casati, B. V. Chirikov, F. M. Izrailev, and J. Ford, *Stochastic Behavior in Classical and Quantum Hamiltonian Systems Lect. Notes Phys.* **90**, 334 (1979).
- [25] D. R. Grempel, R. E. Prange, and S. Fishman, *Phys. Rev. A* **29**, 1639 (1984).
- [26] S. Aubry and G. André, *Ann. Israel. Phys. Soc.* **3**, 133 (1980).
- [27] D. Witthaut, T. Salger, S. Kling, C. Grossert, and M. Weitz, *Phys. Rev. A* **84**, 033601 (2011).
- [28] T. Salger, C. Grossert, S. Kling, and M. Weitz, *Phys. Rev. Lett.* **107**, 240401 (2011).
- [29] S. L. Zhu, B. Wang, and L. M. Duan, *Phys. Rev. Lett.* **98**, 260402 (2007).
- [30] It is interesting to notice that this type of wave-packet dynamics may exist in the square lattice only in the presence of a real (charged particles) or artificial (charge neutral particles) magnetic field normal to the lattice plane [21].
- [31] M. Snoek and W. Hofstetter, *Phys. Rev. A* **76**, 051603(R) (2007).
- [32] O. Peleg, G. Bartal, B. Freedman, O. Manela, M. Segev, and D. N. Christodoulides, *Phys. Rev. Lett.* **98**, 103901 (2007).
- [33] A. Szameit, M. C. Rechtsman, O. Bahat-Treidel, and M. Segev, *Phys. Rev. A* **84**, 021806(R) (2011).
- [34] S. Bittner, B. Dietz, M. Miski-Oglu, P. Oria Iriarte, A. Richter, and F. Schäfer, *Phys. Rev. B* **82**, 014301 (2010).